Immunoproteasome Inhibition

International Edition: DOI: 10.1002/anie.201506631
German Edition: DOI: 10.1002/ange.201506631

# Selective Inhibition of the Immunoproteasome by Structure-Based Targeting of a Non-catalytic Cysteine

*Christian Dubiella,* Regina Baur, Haissi Cui, Eva M. Huber, and Michael Groll**

*Dedicated to Professor Luis Moroder on the occasion of his 75th birthday*

***Abstract:*** *Clinically applied proteasome inhibitors induce cell death by concomitant blockage of constitutive and immunoproteasomes. In contrast, selective immunoproteasome inhibition is less cytotoxic and has the potential to modulate chronic inflammation and autoimmune diseases. In this study, we rationally designed decarboxylated peptides that covalently target a non-catalytic cysteine of the immunoproteasome subunit β5i with α-chloroacetamide-containing sidechains. The enhanced isoform specificity decreased cytotoxic effects and the compound suppressed the production of inflammatory cytokines. Structure-based optimization led to over 150-fold selectivity for subunit β5i over β5c. This new compound class provides a promising starting point for the development of selective immunoproteasome inhibitors as potential anti-inflammatory agents.*

Core particles (CPs) of the proteasome degrade the majority of intracellular proteins and represent essential elements for cell function and survival.[1] While the constitutive proteasome (cCP) is expressed ubiquitously as a central proteolytic machinery, its immunomodulatory isoform, the immunoproteasome (iCP), is predominantly found in cells associated with the immune system.[2] During inflammatory states, iCPs influence the production of cytokines and alter antigen processing, thereby facilitating immune responses.[2] The FDA-approved CP inhibitors bortezomib and carfilzomib (CFZ) block the catalytically active β5 subunits of the cCP (β5c) and iCP (β5i/LMP7) equally.[3] However, simultaneous inhibition of β5c and β5i or combined blockage of other proteolytic subunits (β1i/LMP2, β1c, β2i/MECL1, β2c) induces cytotoxicity, which limits the clinical application of both drugs to the treatment of blood cancer.[4] In contrast, the agent ONX 0914 (PR-957) avoids cytotoxic effects by predominantly blocking β5i. This compound was shown to attenuate the progression of multiple sclerosis and rheumatoid arthritis in mouse models.[5,6] β5i is thus a promising therapeutic target for chronic inflammation and autoimmune disorders.[7] ONX 0914 displays an approximately ten-fold preference for β5i versus β5c owing to an optimized peptide backbone composition.[5] Enhanced binding affinity is achieved through an epoxyketone electrophile that reacts irreversibly with the active-site nucleophile Thr1 (Scheme S1).[8] However, reactive C-terminal warheads have the potential to co-inhibit β5c as well, since the mechanism of proteolysis is the same for all proteasomal active sites. In an attempt to find new target residues that are independent from the proteasomal active site, we followed a structure-guided approach for the design of β5i-specific inhibitors without a C-terminal warhead. By targeting a non-catalytic cysteine as a compensating anchor residue, we aimed to retain sustained covalent binding. The same concept is successfully exploited by inhibitors against various kinases,[9] G-proteins,[10] and the yβ2 subunit[11] of the yeast proteasome (yCP). Structural superposition of the murine subunits mβ5c and mβ5i in combination with sequence alignments highlight Cys48 as a strictly conserved nucleophilic residue that is exclusively found in β5i (Figure 1).[8]

Cys48 is located at a positively charged α-helix dipole, which has the potential to lower the p$K_a$ value of the thiol group, thereby increasing its nucleophilicity. Furthermore,

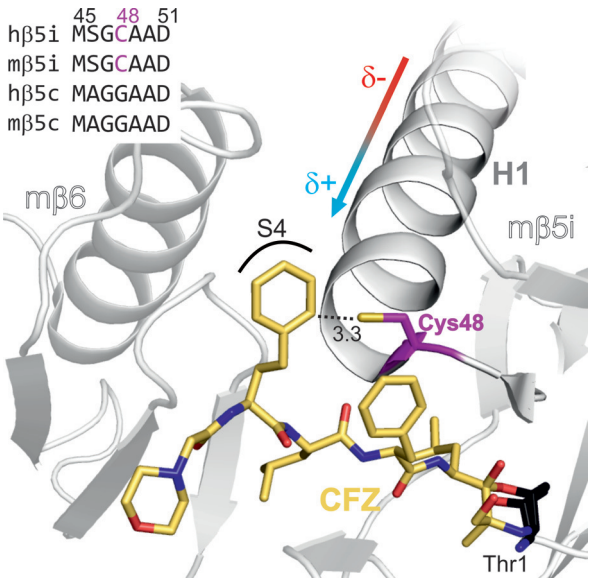


***Figure 1.*** Structural superposition of the murine subunits mβ5i and mβ6 (PDB ID: 3UNH)[8] with CFZ (yellow) bound to Thr1 (black) of subunit yβ5 of yCP (PDB ID: 4QW4).[12] The homophenylalanine P4 residue of CFZ occupies the specificity pocket S4 and is positioned in proximity to Cys48 (magenta, 3.3 Å) of mβ5i. The positively charged N-terminal end of the α-helix dipole H1 points at Cys48. The sequence alignment of β5i and β5c shows Cys48 highlighted in magenta (h = human, m = mouse; upper left corner).

[*] C. Dubiella, R. Baur, H. Cui, Dr. E. M. Huber, Prof. Dr. M. Groll
Center for Integrated Protein Science Munich (CIPSM)
Department of Chemistry, Technische Universität München
Lichtenbergstrasse 4, 85748 Garching (Germany)
E-mail: christian.dubiella@mytum.de
michael.groll@tum.de

Supporting information for this article is available on the WWW under http://dx.doi.org/10.1002/anie.201506631.

  

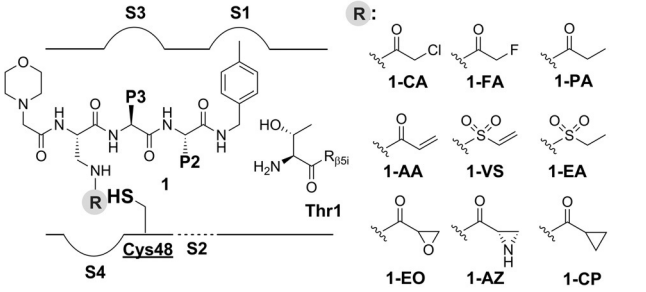


| Compound | P3 | P2 | $IC_{50}$ β5i [μM] | $IC_{50}$ β5c [μM] | $IC_{50}$ β5c/β5i[a] |
|---|---|---|---|---|---|
| 1-CA |  |  | 1.24 ± 0.35 | 11.24 ± 2.59 | 9 |
| 1-PA |  |  | 24.23 ± 3.50 | 29.05 ± 8.85 | 1.2 |
| 2-CA |  | 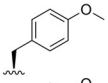 | 6.65 ± 0.27 | > 500 | > 75 |
| 3-CA |  | 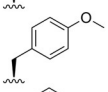 | 2.53 ± 0.56 | 18.27 ± 5.58 | 7 |
| 4-CA |  |  | 0.64 ± 0.14 | > 100 | > 150 |

***Figure 2.*** Schematic representation of the substrate binding channel of β5i with the specificity pockets S1–S4 and Cys48 (underlined). The CFZ-derived decarboxylated peptides **1** contain distinct P4 side-chain electrophiles (R, gray): α-chloroacetamide (**1-CA**), α-fluoroacetamide (**1-FA**), acrylamide (**1-AA**), vinyl sulfonamide (**1-VS**), epoxide (**1-EO**), and aziridine (**1-AZ**). Corresponding non-reactive controls: propionamide (**1-PA**), ethylsulfonamide (**1-EA**), cyclopropanamide (**1-CP**). A complete list of compounds, including half-maximal inhibitory concentration ($IC_{50}$) values, can be found in the supporting information (Tables ST1–3). The lower panel shows the α-chloroacetamides **1-CA**–**4-CA** with their corresponding P2 and P3 residues and the control, **1-PA**. The in vitro $IC_{50}$ values were determined by using purified human iCP or cCP. [a] A high $IC_{50}$ β5c/β5i ratio indicates selectivity for β5i.

Cys48 participates in forming the substrate binding channel of β5i by partially shaping the S2 and S4 pockets. According to structural superpositions, it is accessible via the P4 side chains of tetrapeptides (Figure 1). Consequently, we initiated our inhibitor design by exchanging the P4 residue of CFZ with L-2,3-diaminopropionic acid (Dap). Dap suits the steric requirements of S4 and allows the late-stage introduction of electrophiles owing to its side-chain amino function (Figure 2).

The CFZ-inspired peptide backbone was prepared by solid-phase peptide synthesis using the Fmoc strategy and was C-terminally capped with the previously described 4-methylbenzyl amine.[13,14] In the final step, we introduced various electrophiles by utilizing the corresponding acid chlorides, *N*-hydroxysuccinimide esters, or carboxylic acids in amide coupling reactions. This straightforward synthesis was used to generate a set of decarboxylated peptides with diverse side-chain electrophiles that were shown to be suitable for targeting soft thiol nucleophiles (**1-CA**, **1-FA**, **1-AA**, **1-VS**, **1-EO**, and **1-AZ**; Figure 2).[9] As controls, we prepared their unreactive congeners **1-PA**, **1-EA**, and **1-CP** (Figure 2).

Our initial screening efforts using human iCP and cCP showed that sulfonamide compounds (**1-VS**, **1-EA**) are slightly selective for β5c, whereas amide-bond-connected electrophiles (**1-CA**, **1-FA**, **1-AA**, **1-EO**, **1-AZ**) displayed a preference for β5i (Table ST1 and Figure S1 in the Supporting Information). The most potent electrophile in the screen was **1-CA**, which showed substantial activity against β5i ($IC_{50}$ = 1.24 μM, Figure 2). This is in agreement with studies that propose α-chloroacetamides for sustained targeting of non-catalytic cysteines.[10,15] Despite the unselective peptide backbone of **1-CA**, it displayed nine-fold selectivity for β5i (β5c/β5i = 9), which is comparable to that of ONX 0914 (β5c/β5i ≈ 10).[5] Importantly, **1-CA** was inactive against the subunits β1c, β1i, β2c, and β2i ($IC_{50}$ > 100 μM, Table ST2). The more stable **1-FA**, as well as the unreactive congener **1-PA**, showed significantly decreased $IC_{50}$ values compared to **1-CA**, and both blocked the activity of β5i ($IC_{50}$ = 36.25 μM and 24.23 μM, respectively) and β5c ($IC_{50}$ = 43.84 μM and 29.05 μM, respectively) to the same extent (β5c/β5i = 1.2, Figure 2 and Table ST1). These findings indicate that the β5i binding affinity originates from the α-chloroacetamide electrophile forming a covalent thioether with Cys48 (Scheme S2).

Next, we aimed to assess the covalent binding mode of **1-CA** by X-ray analysis. Since mammalian iCPs are challenging to crystallize, we mimicked the S4 pocket of β5i by replacing Gly48 of the yeast proteasome subunit yβ5 with Cys48 in a plasmid-shuffling procedure (Figure S3a). Subsequent crystallization and structure elucidation of the yβ5G48C mutant yCP (2.8 Å resolution, $R_{free}$ = 20.1%, PDB ID: 5CGF, Table ST4) revealed an orientation of Cys48 identical to that observed in iCP from mouse. In addition, elucidation of the yβ5G48C:ONX 0914 complex structure (2.8 Å resolution, $R_{free}$ = 20.6%, PDB ID: 5CGI) showed a conformation of the ligand analogous to that observed in mβ5i (Figure S4, S5). Strikingly, soaking of yβ5G48C yCP crystals with **1-CA** followed by X-ray analysis (2.9 Å resolution, $R_{free}$ = 23.1%, PDB ID: 5CGG) displayed the ligand exclusively bound to the mutant yβ5 subunit. **1-CA** occupied the substrate binding channel by adopting an antiparallel β-sheet in a similar manner to known inhibitors that are based on decarboxylated peptides.[13,14] In fact, the structure revealed continuous electron density connecting the acetamide function of the P4 side chain of **1-CA** to the thiol group of the introduced Cys48 (Figure 3a). This linkage confirms a covalent mode of action and explains the nine-fold selectivity of **1-CA** for β5i. In contrast, soaking of wild-type yCP crystals as a model for cCP showed empty yβ5 substrate channels, thus emphasizing the importance of Cys48 for **1-CA** binding.

Based on these results, we optimized the peptidic backbone to improve β5i selectivity. As a starting point, we used the peptide composition of ONX 0914 as a molecular blueprint and generated **2-CA** (Figure 2 and Table ST2). Unexpectedly, **2-CA** showed decreased potency against human β5i ($IC_{50}$ = 6.65 μM) and did not bind to the yβ5G48C mutant in soaking experiments. To understand this drop in potency, we compared the binding mode of ONX 0914 with that of **1-CA** and found pronounced differences: the structure of ONX 0914 bound to yβ5G48C revealed a distinct orientation of the P2-TyrOMe that facilitates attractive sulfur–arene interactions with Cys48.[16,17] In contrast, the P2-Phe of **1-CA** is displaced by the P4 side chain, which covalently binds to Cys48, thereby restricting the S2 pocket. To probe the

  

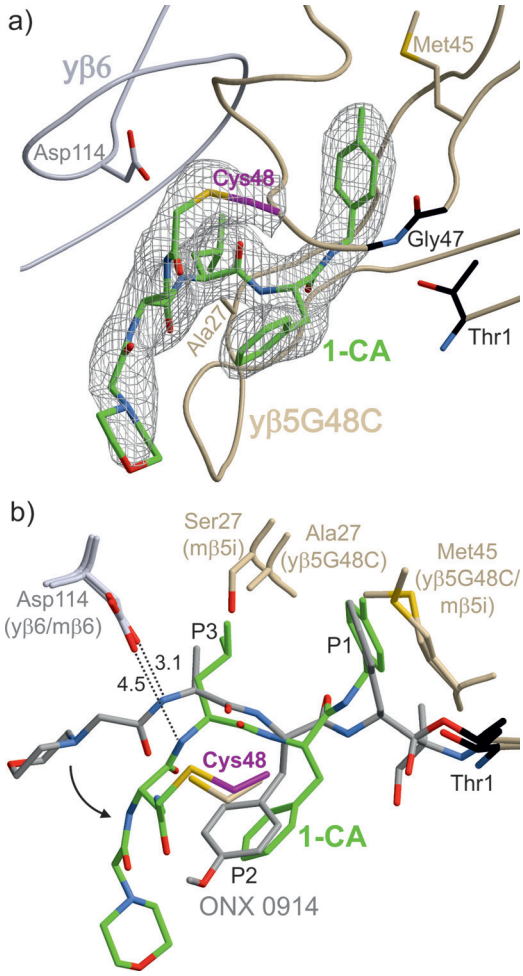


***Figure 3.*** X-ray analysis for the binding of **1-CA** to the yβ5G48C mutant (PDB ID: 5CGG). a) The $2F_o-F_c$ electron density map (gray mesh, contoured at 1σ, 2.9 Å resolution) depicts **1-CA** (green) bound to Cys48 (magenta) of subunit yβ5G48C (beige) with the active-site nucleophile Thr1 (black), oxyanion hole amide of Gly47 (black), and Asp114 of yβ6 (gray). b) Structural superposition of **1-CA** (green) and ONX 0914 (gray) bound to yβ5G48C and to mβ5i (PDB ID: 3UNF), respectively. The P1–P3 sites of the ligand and residues of subunits yβ5, mβ5i (beige), as well as yβ6 and mβ6 (gray), are shown, including distances in Å (black dashed lines). The movement of **1-CA** compared to ONX 0914 is illustrated by a black arrow.

isolated impact of P2-TyrOMe of **2-CA**, we generated **3-CA** (Figure 2, Table ST2). This compound showed inferior β5i-binding affinity ($IC_{50}=2.53$ μM) compared to that of **1-CA** ($IC_{50}=1.24$ μM), thus demonstrating a minor contribution from the S2 pocket. Taken together, these results suggest that the P3 site has a greater influence on potency. Remarkably, the P3-Leu of **1-CA** only incompletely occupies the S3 pocket, which displaces the residual backbone towards subunit β5 (Figure 3b). Therefore, the binding of **1-CA** solely depends on interactions with β5, while the peptide backbone of ONX 0914 is additionally stabilized by Asp114 of β6 (Figure 3b and Figure S6). Since subunit β6 is identical in cCP and iCP, the design of **1-CA** is advantageous owing to an absence of interactions with β6. To test whether the shift of **1-CA** towards β5 is caused by the short Dap spacer, we extended the P4 side chain by replacing Dap with the more flexible L-2,4-diaminobutyric acid (Dab) to give **1-Dab-CA** (Table ST3). However, this resulted in a ten-fold decreased activity against β5i ($IC_{50}=13.07$ μM), thus indicating that the conformationally constrained Dap already has the optimal linker size. Our findings imply that ligand stabilization in the S3 pocket is crucial for the correct positioning of the adjacent P4-α-chloroacetamide. In a similar fashion, the selectivity of ONX 0914 is mainly generated through interactions of the P1-Phe with the S1 pocket, which align the C-terminal warhead for nucleophilic attack of Thr1.[8]

As a result, we focused on the most prominent differences between the S3 pockets of human β5i and β5c by applying homology modelling combined with sequence alignments (Figure S3b). The strictly conserved substitution of Ala27 (β5c) by Ser27 (β5i) alters the polarity and size of the S3 pocket (Figure 3b).[8] To address this observation, we generated **4-CA** (Figure 2), in which an Asn in the P3 position allows enhanced hydrogen bonding to Ser27. Indeed, **4-CA** exhibited up to 150-fold selectivity for β5i ($IC_{50}=0.64$ μM) over β5c, whereas the unreactive congener **4-PA** proved to be only seven-fold selective for β5i, with significantly decreased potency ($IC_{50}=29.29$ μM; Table ST2). These observations confirm that the nature of the P3 residue and its stabilization are crucial for appropriate ligand binding. We could achieve β5i selectivity by exclusively modifying the P3 position. This is in contrast to Thr1-targeting inhibitors, which primarily rely on P1-residue stabilization.

Next, we aimed to examine the effect of **1-CA** and **4-CA** in cell-culture assays. Our prime focus was to analyze their inhibitory and cytotoxic profiles, as well as their impact on the production of inflammatory cytokines. By using a luminogenic substrate assay, we first determined the in vivo $IC_{50}$ values with lysate from THP-1 cells, which constitutively express high levels of iCP.[18] Both **1-CA** ($IC_{50}=2.83$ μM) and **4-CA** ($IC_{50}=3.55$ μM) substantially blocked β5 activity compared to the unreactive control **1-PA** ($IC_{50}=36.69$ μM), which is in line with the in vitro data (Figure S7a). Second, we investigated the effects on cell viability. Concentrations of up to 10 μM of **1-CA** and **4-CA** had no effect on the cells (Figure S7b). Finally, we evaluated the possible application of **1-CA** as an anti-inflammatory agent based on the favorable pharmacokinetics of the CFZ backbone. We examined its effect on the inflammation markers tumor necrosis factor alpha (TNF-α) and interleukin 6 (IL-6) by using an enzyme-linked immunosorbent assay (ELISA). **1-CA** indeed suppressed the production of TNF-α and IL-6 in a dose-dependent manner. 10 μM of **1-CA** reduced IL-6 levels substantially without causing cell death, and 25 μM led to a reduction in TNF-α production (Figure 4, Figure S8). This reduction in cytokine production has similarly been described for ONX 0914.[5]

In summary, our study describes the first immunoproteasome inhibitor that acts independently of the active-site nucleophile Thr1. Commencing with structural bioinformatics, we identified Cys48 in β5i as an isoform-specific nucleophilic residue that is accessible to tetrapeptides. For this purpose, we synthesized decarboxylated peptides and performed an electrophile screening procedure, which revealed the α-chloroacetamide warhead of **1-CA** as the best option. In addition, we optimized the P3 site based on

  

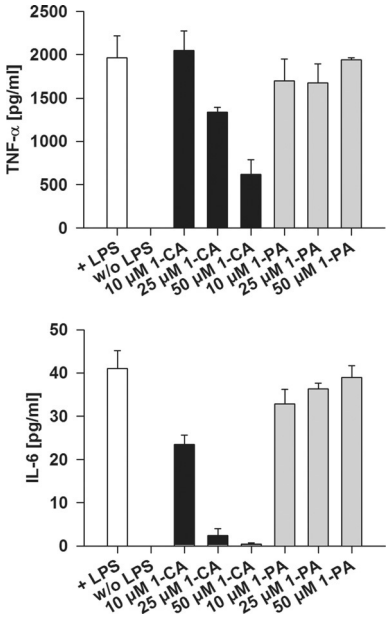


***Figure 4.*** Quantification of the cytokines TNF-α and IL-6 produced by THP-1 cells after exposure to lipopolysaccharides (LPS, controls as white bars) and treatment with various concentrations (10–50 μM) of **1-CA** (black bars) and **1-PA** (gray bars) as a negative control by ELISA. **1-CA** suppresses IL-6 and TNF-α production in a dose-dependent manner. Data are shown as the mean + standard error of the mean ($n = 4$).

structural information, thereby underlining its impact on β5i selectivity for this new concept of inhibition. Cell-based assays confirmed that **1-CA** blocks the activity of β5 at concentrations below the induction of cytotoxicity, thereby suppressing the production of cytokines such as TNF-α and IL-6. Taken together, these properties highlight this new class of compounds as a starting point for the development of selective immunoproteasome inhibitors as potential anti-inflammatory agents.

## Acknowledgements

This work was funded by SFB 1035/A2. We thank Richard Feicht for experimental support and the staff of PXI of the Paul Scherrer Institute, Swiss Light Source (Villigen, Switzerland) for help with data collection.

**Keywords:** drug design · immunology · immunoproteasome · selective inhibitors · structure–activity relationships

**How to cite:** *Angew. Chem. Int. Ed.* **2015**, *54*, 15888–15891
*Angew. Chem.* **2015**, *127*, 16116–16120

[1] A. Hershko, A. Ciechanover, *Annu. Rev. Biochem.* **1998**, *67*, 425–479.
[2] M. Groettrup, C. J. Kirk, M. Basler, *Nat. Rev. Immunol.* **2010**, *10*, 73–78.
[3] S. D. Demo, C. J. Kirk, M. A. Aujay, T. J. Buchholz, M. Dajee, M. N. Ho, J. Jiang, G. J. Laidig, E. R. Lewis, F. Parlati, et al., *Cancer Res.* **2007**, *67*, 6383–6391.
[4] a) F. Parlati, S. J. Lee, M. Aujay, E. Suzuki, K. Levitsky, J. B. Lorens, D. R. Micklem, P. Ruurs, C. Sylvain, Y. Lu, et al., *Blood* **2009**, *114*, 3439–3447; b) D. Niewerth, J. van Meerloo, G. Jansen, Y. G. Assaraf, T. C. Hendrickx, C. J. Kirk, J. L. Anderl, S. Zweegman, G. J. L. Kaspers, J. Cloos, *Biochem. Pharmacol.* **2014**, *89*, 43–51; c) A. C. Mirabella, A. A. Pletnev, S. L. Downey, B. I. Florea, T. B. Shabaneh, M. Britton, M. Verdoes, D. V. Filippov, H. S. Overkleeft, A. F. Kisselev, *Chem. Biol.* **2011**, *18*, 608–618; d) M. Britton, M. M. Lucas, S. L. Downey, M. Screen, A. A. Pletnev, M. Verdoes, R. A. Tokhunts, O. Amir, A. L. Goddard, P. M. Pelphrey, et al., *Chem. Biol.* **2009**, *16*, 1278–1289.
[5] T. Muchamuel, M. Basler, M. A. Aujay, E. Suzuki, K. W. Kalim, C. Lauer, C. Sylvain, E. R. Ring, J. Shields, J. Jiang, et al., *Nat. Med.* **2009**, *15*, 781–787.
[6] M. Basler, S. Mundt, T. Muchamuel, C. Moll, J. Jiang, M. Groettrup, C. J. Kirk, *EMBO Mol. Med.* **2014**, *6*, 226–238.
[7] A. F. Kisselev, M. Groettrup, *Curr. Opin. Chem. Biol.* **2014**, *23*, 16–22.
[8] E. M. Huber, M. Basler, R. Schwab, W. Heinemeyer, C. J. Kirk, M. Groettrup, M. Groll, *Cell* **2012**, *148*, 727–738.
[9] a) Q. Liu, Y. Sabnis, Z. Zhao, T. Zhang, S. J. Buhrlage, L. H. Jones, N. S. Gray, *Chem. Biol.* **2013**, *20*, 146–159; b) T. Zhang, F. Inesta-Vaquera, M. Niepel, J. Zhang, S. B. Ficarro, T. Machleidt, T. Xie, J. A. Marto, N. Kim, T. Sim, et al., *Chem. Biol.* **2012**, *19*, 140–154; c) M. Nacht, L. Qiao, M. P. Sheets, T. St. Martin, M. Labenski, H. Mazdiyasni, R. Karp, Z. Zhu, P. Chaturvedi, D. Bhavsar, et al., *J. Med. Chem.* **2013**, *56*, 712–721; d) M. Hagel, D. Niu, T. St Martin, M. P. Sheets, L. Qiao, H. Bernard, R. M. Karp, Z. Zhu, M. T. Labenski, P. Chaturvedi, et al., *Nat. Chem. Biol.* **2011**, *7*, 22–24; e) F. Solca, G. Dahl, A. Zoephel, G. Bader, M. Sanderson, C. Klein, O. Kraemer, F. Himmelsbach, E. Haaksma, G. R. Adolf, *J. Pharmacol. Exp. Ther.* **2012**, *343*, 342–350; f) I. M. Serafimova, M. A. Pufall, S. Krishnan, K. Duda, M. S. Cohen, R. L. Maglathlin, J. M. McFarland, R. M. Miller, M. Frödin, J. Taunton, *Nat. Chem. Biol.* **2012**, *8*, 471–476.
[10] S. M. Lim, K. D. Westover, S. B. Ficarro, R. A. Harrison, H. G. Choi, M. E. Pacold, M. Carrasco, J. Hunter, N. D. Kim, T. Xie, et al., *Angew. Chem. Int. Ed.* **2014**, *53*, 199–204; *Angew. Chem.* **2014**, *126*, 203–208.
[11] G. Loidl, M. Groll, H.-J. Musiol, L. Ditzel, R. Huber, L. Moroder, *Chem. Biol.* **1999**, *6*, 197–204.
[12] E. M. Huber, W. Heinemeyer, M. Groll, *Structure* **2015**, *23*, 407–417.
[13] C. Blackburn, K. M. Gigstad, P. Hales, K. Garcia, M. Jones, F. J. Bruzzese, C. Barrett, J. X. Liu, T. A. Soucy, D. S. Sappal, et al., *Biochem. J.* **2010**, *430*, 461–476.
[14] a) C. Blackburn, C. Barrett, J. L. Blank, F. J. Bruzzese, N. Bump, L. R. Dick, P. Fleming, K. Garcia, P. Hales, M. Jones, et al., *MedChemComm* **2012**, *3*, 710–719; b) M. Groll, N. Gallastegui, X. Maréchal, V. Le Ravalec, N. Basse, N. Richy, E. Genin, R. Huber, L. Moroder, J. Vidal, et al., *ChemMedChem.* **2010**, *5*, 1701–1705.
[15] a) C. Jöst, C. Nitsche, T. Scholz, L. Roux, C. D. Klein, *J. Med. Chem.* **2014**, *57*, 7590–7599; b) E. Weerapana, G. M. Simon, B. F. Cravatt, *Nat. Chem. Biol.* **2008**, *4*, 405–407; c) N. Brauckhoff, G. Hahne, J. T. H. Yeh, T. N. Grossmann, *Angew. Chem. Int. Ed.* **2014**, *53*, 4337–4340; *Angew. Chem.* **2014**, *126*, 4425–4429.
[16] L. M. Salonen, M. Ellermann, F. Diederich, *Angew. Chem. Int. Ed.* **2011**, *50*, 4808–4842; *Angew. Chem.* **2011**, *123*, 4908–4944.
[17] K. N. Daeffler, H. A. Lester, D. A. Dougherty, *J. Am. Chem. Soc.* **2012**, *134*, 14890–14896.
[18] D. Niewerth, G. J. L. Kaspers, Y. G. Assaraf, J. van Meerloo, C. J. Kirk, J. Anderl, J. L. Blank, P. M. van de Ven, S. Zweegman, G. Jansen, et al., *J. Hematol. Oncol.* **2014**, *7*, 7.

Received: July 17, 2015
Revised: September 15, 2015
Published online: November 13, 2015

  